International Journal of Heat and Mass Transfer 106 (2017) 526–538

Contents lists available at ScienceDirect

International Journal of Heat and Mass Transfer

journal homepage: www.elsevier.com/locate/ijhmt

Multi-scale numerical analysis of flow and heat transfer for a parabolic trough collector

Zhen Tang, Xin-Peng Zhao, Zeng-Yao Li, Wen-Quan Tao *

Key Lab of Thermo-Fluid Science and Engineering of MOE, Xi'an Jiaotong University, Xi'an 710049, China

ARTICLE INFO

Article history:
Received 25 June 2016
Received in revised form 1 September 2016
Accepted 1 September 2016
Available online 13 September 2016

Keywords:
Parabolic trough collector
DSMC
Coupled heat transfer
Multi-scale

ABSTRACT

This paper numerically investigated the coupled flow and heat transfer of a parabolic trough collector (PTC), with the non-uniform heat flux boundary condition on the absorber wall and the rarefied gas effects in the annular vacuum gap being taken into consideration. A fully coupled cross-sectional heat transfer model is established with Direct Simulation Monte Carlo (DSMC) method for the rarefied gas flow and heat transfer in the vacuum annual gap. The PTC tube efficiency can be obtained from the above simulation for a given HTF temperature. Such simulation is conducted for several specified HTF temperature and different efficiency data are obtained. These data are fitted by an equation. This equation is then used to advance the HTF temperature in the axial direction. In such a way a simplified 3D model for the design of a PTC receiver is obtained. Cross-sectional simulation results show that when the gas pressure is less than 0.1 Pa further decrease in pressure makes no further contribution to reduce the heat loss. The effects of periphery non-uniform distribution of heat flux, coating material emissivity, envelope diameter and HTF inlet velocity on the PTC efficiency are discussed. An operation variant is proposed by using the 3D model by which the total PTC tube length can be reduced for a given thermal load.

© 2016 Elsevier Ltd. All rights reserved.

1. Introduction

Parabolic trough collector (PTC) is one kind of solar receivers which are the energy conversion devices by converting solar radiant energy of sunlight focused by the mirrors to thermal energy [1–3]. This solar receiver consists of a stainless absorbing tube and a surrounding annular vacuum space with a glass envelope. The stainless tube, with a selective emissivity coating on the surface, absorbs the radiant energy transmitting through the glass tube, converts it to thermal energy and transfers the thermal energy to the heat transfer fluid (HTF) flowing within the tube. The heated HTF flows to a heat accumulator and stores heat in it. After that, the stored heat is used to produce high temperature steam in a steam generator, which would drive a conventional turbine-generator to produce electricity. Now the efficiencies of the steam generator (about 98%), steam turbine (about 88%) and electric generator (about 95%) are quite high and stable because the input conditions of these machines are fixed by adopting the heat accumulator. But the efficiency of PTC is not high (about 36%) and changes a lot because of the effects of various factors [4] shown in Fig. 1. At the present time the whole solar system efficiency is still at a low level (about 30%) [5], mainly because the PTC's efficiency is low. So increasing the PTC's efficiency plays an important role in making the solar electricity generation system being more compatible with fuel-power plant.

In order to gain a high efficiency of the PTC, the manufacturers adopt some advanced techniques to reduce heat loss from the absorber tube to the environment, such as using a low thermal emittance cermet selective coatings on the absorber and adopting a vacuum annular glass envelope surrounding the absorber tube. Usually, the annular gap between the absorber tube and the glass envelope is kept at a high vacuum. The selective coatings have the characteristics of high absorptivity ($\alpha = 0.98$) and low emittance ($\varepsilon \leqslant 0.15$) which will reduce the self-thermal radiation of the absorber. The convection heat transfer in the gap is mainly affected by the gas pressure in the gap [6]. Usually the pressure is designed to be lower than 0.001 Pa. On the other hand, the absorber tubes are heated by non-uniform heat flux resulted from the concentration of the parabolic trough [2], which leads to the non-uniform distribution temperature of the tube. So the emittance selective coatings of cermet, the gas pressure in the annular gap and the non-uniform heat flux on the tube are the major factors affecting the efficiency of the PTC [7,8]. Apart from the above-mentioned three factors, the inlet temperature and volume flow rate of HTF, solar radiation, ambient air temperature, and

* Corresponding author.
E-mail address: wqtao@mail.xjtu.edu.cn (W.-Q. Tao).

http://dx.doi.org/10.1016/j.ijheatmasstransfer.2016.09.002
0017-9310/© 2016 Elsevier Ltd. All rights reserved.

Nomenclature

D	diameter (m)
E	energy (J)
c_p	heat capacity (kJ/(kg·K))
q	heat flux (W/m)
h	heat transfer coefficient (W/(m^2·K))
Kn	Knudsen number
d_{mol}	molecule diameter (m)
Nu	Nusselt number
P	pressure (Pa)
Pr	Prandtl number
Re	Reynolds number
T	temperature (K)
t	time (s)
k	thermal conductivity (W/(m·K))
V	velocity (m/s)

Greek symbols

δ	absorber tube thickness (m)
α	absorptivity
κ	Boltzmann constant
ρ	density (kg/m^3)
ε	emittance
ν	kinematic viscosity (mm^2/s)
$\bar{\lambda}$	mean free path (m)

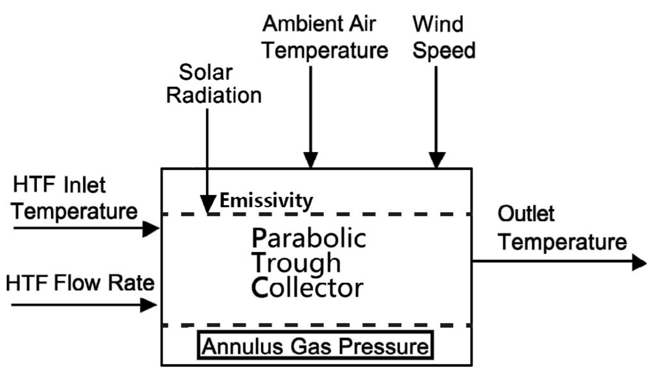

Fig. 1. Black box model of the heat collector element.

wind speed have their affections on the efficiency of a PTC as well, as shown in Fig. 1. While the outlet temperature of the HTF is the production of a PTC.

In order to investigate the effects of the above factors numerical simulation and experimental measurement have been widely conducted. The results of experimental studies are often expressed by correlation or fitting formulas. In this regard, the investigation conducted in [6] is quite representative, and is introduced a bit in detail below. The following assumptions are made in the paper: (1) for the temperature difference to determine the convection heat transfer between the HTF and the absorber wall, the HTF temperature is the fluid bulk temperature; (2) the flow is laminar with a uniform flux; (3) for the convection heat transfer between the absorber tube and glass envelope, the convection heat transfer coefficient is constant and the temperatures of the absorber tube and glass are kept at different but uniform (The author specifically remind that "At low pressures (<0.0001 torr), the heat transfer may be slightly overestimated."); (4) for the convection heat transfer between the glass envelope and the atmosphere, a long isothermal horizontal cylinder is assumed. A fitting formulas of performance analysis based on the first law of thermodynamics is used in [6] to study all these factors. The heat transfer analysis of a PTC is implemented by the Engineering Equation Solver. Such studies could provide some necessary information for a quick engineering estimation, but could not obtain details of the transfer process which are necessary for further improving the efficiency of a PTC.

A number of studies for which the CFD method were used focus on the inlet temperature and volume flow rate of HTF [9,10]. In [9], a three-dimensional simulation based on finite element method of a PTC using molten salt as HTF was conducted. But the authors did not simulate the flow and heat transfer in the annulus. In [10], the authors analyzed the effect of the utilization of internal finned tubes with computational fluid dynamics. Results showed an improvement potential in parabolic trough solar plant efficiency by the application of internal finned tubes.

For the solar radiation, a coupled simulation method based on Monte Carlo Ray Trace (MCRT) and finite volume method (FVM) is established to solve the coupled heat transfer problem of radiation, heat conduction and convection in the PTC in [11,12]. The numerical results, especially the heat flux distributions along the periphery of the glass tube , were in good agreement with experimental data of LS2 PTC of Sandia National Laboratory [13], proving that the model and method proposed in [2] is feasible and reliable. In [14] a detailed one dimensional view factors for a short annulus is presented for the radiative heat transfer.

For the annulus gas pressure, some simulations by the direct simulation of Monte Carlo (DSMC) model used uniform wall temperature boundary [15,16]. A unified two-dimensional numerical model was used for the coupled heat transfer process in a PTC and the effects of tube diameter ratio were numerically analyzed [17]. Considering the very non-uniform heat flux distribution along the tube periphery, helical screw-tape inserts was proposed to homogenize the absorber tube temperature distribution and improve the working condition of the PTC tube [18]. In [19], DSMC was used to analyze the conduction heat loss from a PTC with controlled pressure within the annular gap. For the effects of ambient air temperature and wind speed, numerical simulations for the outside convective heat transfer were used in [20–23]. FVM was used to solve the governing equations and the SIMPLE algorithm was employed to deal with the coupling between velocity and pressure in [22,23]. A numerical study based on Large Eddy Simulations was carried out to characterize the wind loads and heat transfer coefficients [22,23]. In reality, the heat transferred by rarefied gas in the annular gap is coupled with both the heat transfer in the absorber tube and that outside the glass envelope.

Most these works used the uniform or constant solar flux assumption along the tube periphery and many correlations based on a uniform or constant temperature assumption, thus making the simulation of the entire heat transfer processes being not fully coupled. The aim of this paper is to provide a complete coupled heat transfer model, from heat transfer of HTF within the inner tube to the heat transfer from envelope to the atmosphere to study the affecting factors of PTC, with major focus being put on the influence of the non-uniform heat flux and rarefied gas heat transfer in the annual gap by DSMC. In the following presentation the physical model and numerical method will be briefly introduced, then numerically simulated results will be provided in details, including cross-sectional parameter distributions and axial-wise variation of HTF temperature. Discussion on the effects of a number of factors on PTC efficiency will be presented. Finally, some conclusions will be withdrawn.

2. Physical model and numerical method

2.1. Physical model

In order to compare the resulted data between the simulations and experiments, the Schott receiver is chosen as the physical model for the simulations, which was tested on the LS-2 collector module test platform at Sandia National Laboratories (SNL) [5]. A 2-D schematic diagram of the receiver is illustrated in Fig. 2. All the parameters are listed in Table 1.

For the convenience of analysis and focusing our attention on the major factors, following assumption are made:

(1) The entire heat transfer process is in steady state;
(2) The convection heat transfer within the tube is in the fully developed region;
(3) The conductive resistance through the selective coating is neglected;
(4) The glass envelop is opaque to thermal radiation (in the infrared spectrum) and is gray and diffuse.

A complete coupled flow and heat transfer model of the receiver should contain the following heat transfer processes: convection heat transfer between the HTF and absorber tube $q_{1-2,conv}$, the solar energy flux distribution on the absorber wall which is mainly transferred through heat conduction $q_{2-3,cond}$, heat transfer in the evacuated annular gap through the rarefied gas $q_{3-4,conv}$, thermal radiation heat transfer from the outer surface of the absorber tube to the inner surface of glass envelope $q_{3-4,rad}$, heat conduction through glass envelope wall $q_{4-5,cond}$, thermal radiation heat transfer from the glass envelope to sky $q_{5-7,rad}$ and the convection heat transfer from the glass envelope to the atmosphere $q_{5-6,conv}$. All these heat transfer processes will be analyzed in the present model. Considering that the convective heat transfers within a tube and across a tube have been well investigated in heat transfer community, experimental results for average or local Nusselt number will be directly used. In practical situation wind speed across a PTC varies with time, hence several representative values of wind speed will be adopted to analyze the outside convection effect. Fig. 3 shows the grid system of a cross section to calculate the flow and heat transfer (both convection and surface radiation) mentioned above.

Table 1
Parameters.

Items	Units	Value
Heat transfer fluid (HTF)		*Therminol VP-1*
Inlet temperature of HTF ($T_{1,HTF}$)	K	363.15–613.15
Inlet velocity of HTF ($V_{1,HTF}$)	m/s	0.861–3.444
Absorber inner diameter (D_2)	mm	66
Absorber outer diameter (D_3)	mm	70
Absorber thermal conductivity (k_{23})	W/(m·K)	$0.013 * T_{23} + 15.2$
Coating emittance (ε_3)		$T_3 * 3.25 * 10^{-4} - 0.06478$
Glass emittance (ε_4)		0.92
Pressure in annular space (P_{34})	Pa	0.01–10
Glass inner diameter (D_4)	mm	109
Glass outer diameter (D_5)	mm	115
Glass thermal conductivity (k_{45})	W/(m·K)	1.04
Aperture width	m	5
Receiver (HCE) length	m	1
Optical efficiency		74.13%
Direct normal Irradiation(DNI)	W/m^2	940
Air temperature (T_6)	K	298.15
Effective sky temperature (T_7)	K	290.15
Wind velocity	m/s	1–8.9

2.2. Numerical method

In this section the above-mentioned heat transfer processes will be described on how to determine the heat flux through each process.

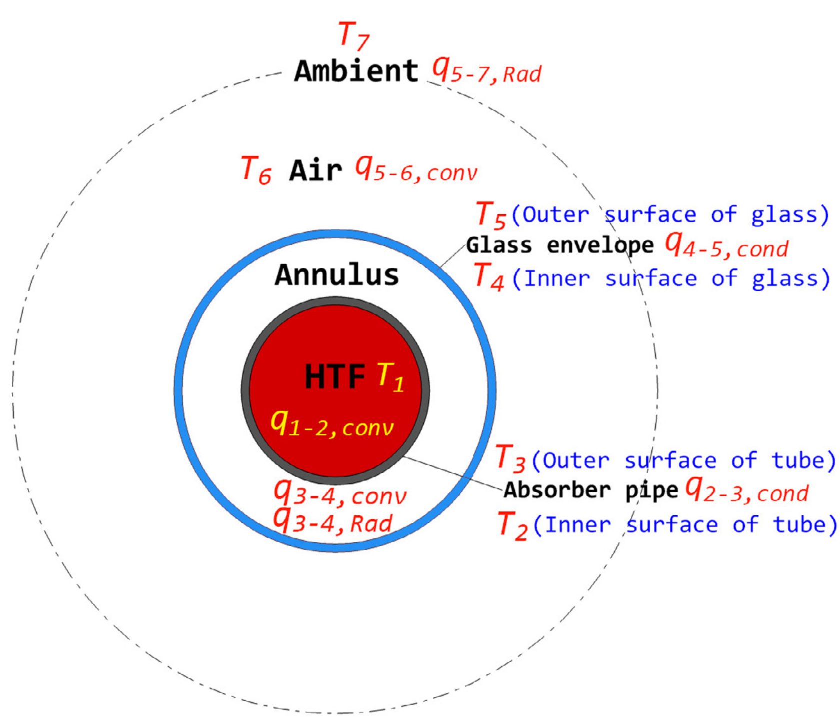

Fig. 2. The simplified 2-D schematic diagram of a PTC.

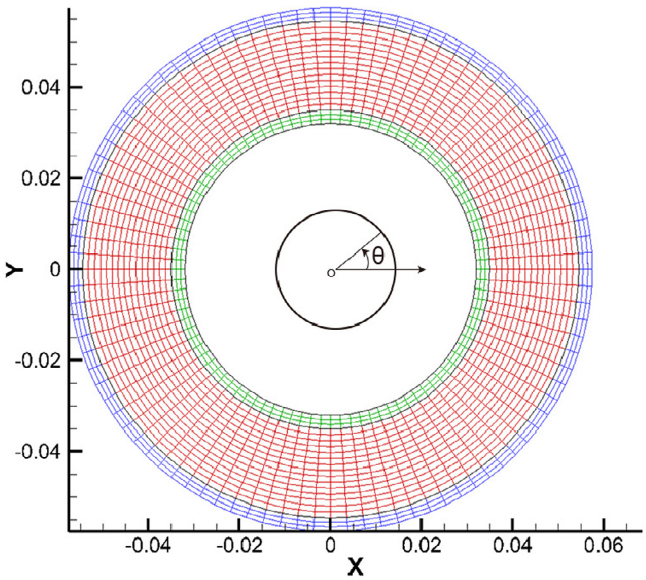

Fig. 3. Calculation gird.

2.2.1. Convection heat transfer between the HTF and the absorber

When the PTC is working at typical operating conditions, the flow in a PTC is well within the turbulent region [6]. From the Newton's low of cooling, the convection heat transfer flux of the HTF can be calculated

$$q_{1-2,conv} = h_{1-2}\pi D_2(T_2 - T_1) \tag{1}$$

$$h_{1-2} = \frac{\lambda_1}{D_2} Nu_{D2} \tag{2}$$

Gnielinski's equation [24] is used to predict Nu_{D2}:

$$Nu_{D2} = \frac{f_2/8 * (Re_{D2} - 1000)Pr_1}{1 + 12.7\sqrt{f_2/8}(Pr_1^{2/3} - 1)} \tag{3}$$

$$f_2 = \sqrt{1.82 \lg Re_{D2} - 1.64} \tag{4}$$

2.2.2. Conduction heat transfer through the absorber wall

Fourier's law of conduction through the wall of a hollow cylinder is used.

$$q_{3-2}(\theta) = \lambda_{23}\frac{T_3(\theta) - T_2(\theta)}{\delta} \tag{5}$$

When the tube is in energy balance this conduction heat transfer is equal to the inner wall convection heat transfer.

The thermal conductivity is calculated at the average temperature between the inner and outer surfaces. The thermal conductivity of 316L stainless steel is determined by the following equation [25]:

$$\lambda_{23} = 0.013 * T_{23} + 15.2 \tag{6}$$

2.2.3. Radiation heat transfer from the outer surface of the absorber tube to the inner surface of the glass envelope

Radiation heat transfer occurs between the absorber outer surface and the inner surface of the glass envelop. The "surface-to-surface" radiation needs to be considered. If the two walls are kept at uniform temperatures of T_3 and T_4, respectively, the radiation heat flux between the two long concentric isothermal cylinders can be estimated with the following equation [26]:

$$q_{3-4,rad} = \frac{\sigma\pi D_3(T_3^4 - T_4^4)}{1/\varepsilon_3 + (1-\varepsilon_4)D_3/(\varepsilon_4 D_4)} \tag{7}$$

However, since the heat flux is non-uniform, the temperatures on the walls are not uniform. To study the influence of the non-uniform temperatures on the radiation heat transfer, the cylindrical surface is divided into cells shown in Fig. 3 and direct exchange of radiative energy between different surface cell is calculated as follows.

For any cell on the wall surfaces in Fig. 4,

$$q_{out,i} = \varepsilon_i\sigma T_i^4 + \rho_i q_{in,i} \tag{8}$$

$$dA_i q_{out,i} = \sum_{j=1}^{N} dA_j X_{ji} q_{out,j} \tag{9}$$

where

$q_{out,i}$ is the output radiative energy of the cell i,
$q_{in,i}$ is the sum of input radiative energy of cell i from the glass,
ε_i, ρ_i are the emittance and reflectivity of the cell i,
N is the total number of cells,
dA_i is the area of the cell i, and X_{ji} is the view factor between cell j and i.

$$X_{ij} = \frac{dA_i \cos\theta_i \cos\theta_j}{\pi r^2} \tag{10}$$

$$dA_j X_{ji} = dA_i X_{ij}, \; j = 1, 2, 3, \ldots N \tag{11}$$

$$q_{in,i} = \sum_{j=1}^{N} X_{ij} q_{out,j} \tag{12}$$

$$q_{out,i} = \varepsilon_i\sigma T_i^4 + \rho_i\sum_{j=1}^{N} X_{ij} q_{out,j} \tag{13}$$

It can be written as:

$$J_i = E_i + \rho_i\sum_{j=1}^{N} X_{ij} J_j \tag{14}$$

where J_i and E_i are the effective surface radiation and self-radiation of cell i, respectively.

Fig. 4 shows schematically on the calculation of the view factors in the annular gap where the inner surface and out surface are named as 3 and 4 respectively. It is to be noted that surface 3 is convex, while surface 4 is concave.

In Fig. 4(b),

$$\begin{aligned} & r = \sqrt{r_3^2 + r_4^2 - 2\cdot r_3\cdot r_4\cos(\theta_3 - \theta_4)} \\ & m = PM = r_4\cos(\theta_3 - \theta_4) - r_3 \\ & \cos\varphi_1 = \tfrac{m}{r} \\ & \cos\varphi_2 = \tfrac{r^2 - r_3^2 + r_4^2}{2\cdot r\cdot r_4} \\ & X_{3i,4j} = r_4\cdot\Delta\theta\cdot\cos\varphi_1\cdot\cos\varphi_2/(\pi\cdot r) \end{aligned} \tag{15}$$

In Fig. 4(d),

$$\begin{aligned} & r = 2\cdot PM = 2\cdot r_4\sin\tfrac{(\theta_3-\theta_4)}{2} \\ & \cos\varphi_1 = \cos\varphi_2 = \sin\tfrac{(\theta_3-\theta_4)}{2} \\ & X_{4i,4j} = \Delta\theta/(4\cdot\pi\cdot r) \end{aligned} \tag{16}$$

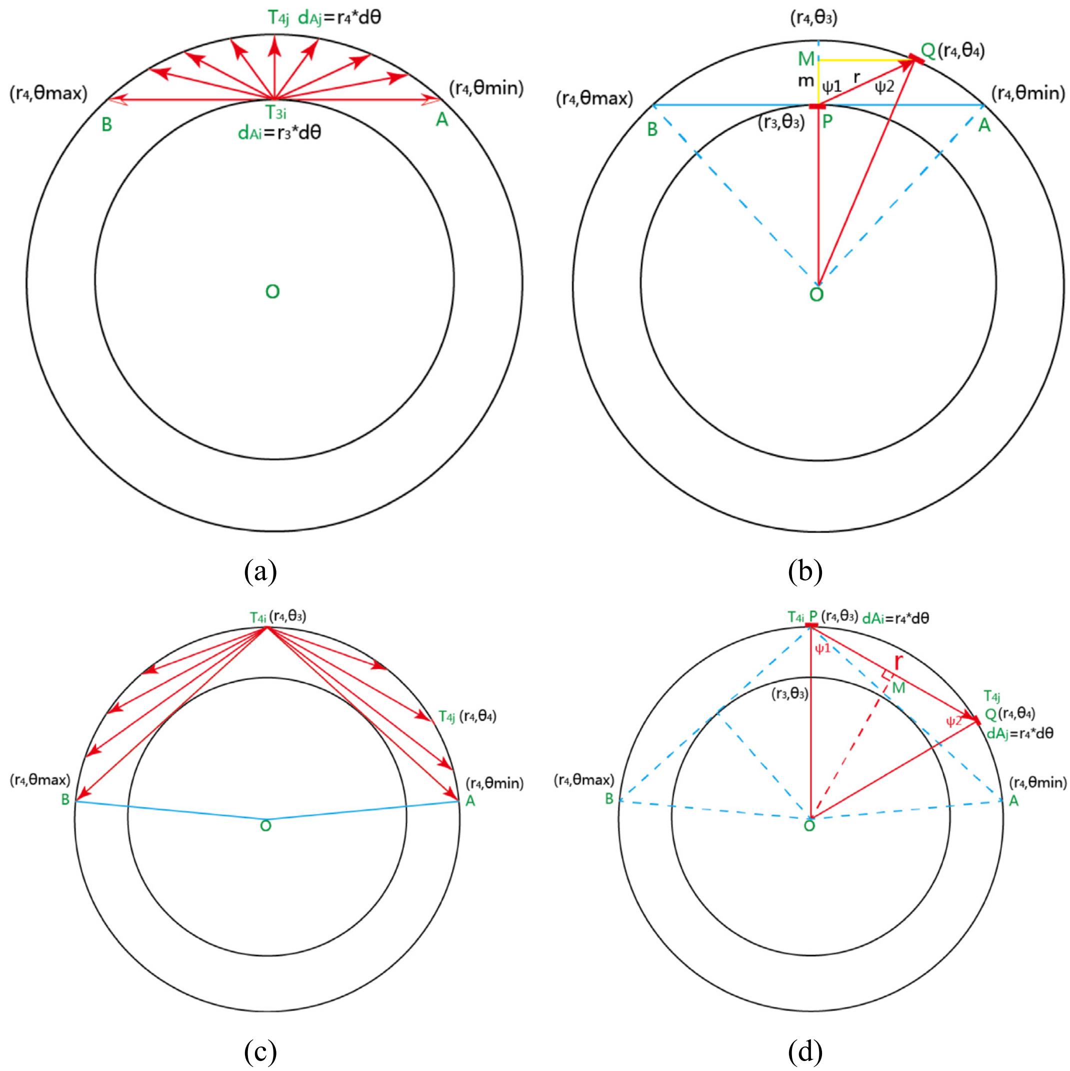

Fig. 4. Schematic diagram of view factor calculation.

2.2.4. Convection heat transfer from the outer surface of the absorber tube to the inner surface of the glass envelope

This is a region occupied by rarefied gas. The flow regime can be characterized by the Knudsen number (Kn) which is evaluated by the mean free path ($\bar{\lambda}$) of gas and the characteristic length of the flow region [27].

$$Kn = \frac{\bar{\lambda}}{R_4 - R_3} \tag{17}$$

$$\bar{\lambda} = \frac{\kappa T_{gas}}{\sqrt{2}\pi d_{mol} P} \tag{18}$$

where P (in Pa) is the absolute pressure in the annular gap.

If the Knudsen number is larger than 0.01, the continuum model is not suitable for the gaseous flow and the heat transfer. Then the status of gas can be described by the Boltzmann equation. Generally, the pressure in the annular gap is kept very low (<0.013 Pa) to reduce the heat losses [28].

In the simulations, the outer boundary radius R_4 = 0.0545 m and the inner boundary radius R_3 = 0.0350 m. The pressure in the gap varies from 0.05 to 100 Pa, and the Knudsen number is 0.03–8.0. So, the gas in annular gap is rarefied. In the present study, the DSMC method is adopted to simulate the rarefied gaseous flow field.

DSMC method is an effective numerical method to simulate the rarefied gaseous flow field [29]. In the method, the movements and collisions of the simulation particles are decoupled. And the macroscopic parameters are obtained by sampling the transient properties of the simulation particles in a domain within a given period. A modified code based on Bird's code "DSMC2A.for" is developed in this paper. The new DSMC code implements a new non-uniform boundary condition. Fully diffuse reflection and variable hard sphere (VHS) model are used in the DSMC method. The implementation of the new boundary condition, i.e. with given wall heat flux determine the wall temperature, is described as follows.

The outer surface of the absorber tube is given by the local heat flux along the periphery and the correspondent local wall temperature, $T_{wall-3}(\theta)$ should be determined. Akhlaghi et al. used Eq. (19) [30]:

$$T_{wall\text{-}3}(\theta)^{new} = T_{wall\text{-}3}(\theta)^{old}\left(1 + RF\frac{q_{wall\text{-}3}(\theta) - \Delta q_{heat}(\theta)}{|\Delta q_{heat}(\theta)| + \varepsilon_0}\right) \tag{19}$$

where the value of relaxation factor RF is recommended <0.03.

Our preliminary simulation found that by using Eq. (19) the convergence speed was severely deteriorated because the range of $q_{Init}(\theta)$ (showed in Fig. 5) is wide and close to zero in some zones. Thus Eq. (19) is modified to accommodate the non-uniform heat flux as follows:

$$T_{wall\text{-}3}(\theta)^{new} = T_{wall\text{-}3}(\theta)^{old}\left(1 + RF\frac{q_{wall\text{-}3}(\theta) - \Delta q_{heat}(\theta)}{(|q_{wall\text{-}3}(\theta)| + |\Delta q_{heat}(\theta)|)/2}\right) \tag{20}$$

$$T_{wall\text{-}4}(\theta)^{new} = T_{wall\text{-}4}(\theta)^{old}\left(1 + RF\frac{q_{wall\text{-}4}(\theta) - \Delta q_{heat}(\theta)}{(|q_{wall\text{-}4}(\theta)| + |\Delta q_{heat}(\theta)|)/2}\right) \tag{21}$$

$$q_{wall}(\theta) = \frac{(\sum E)_{incidence} - (\sum E)_{reflection}}{\Delta t \cdot A} \tag{22}$$

where

θ is the polar coordinate,
q_{wall} is the statistical heat flux gotten by the DSMC code ($= q_{DSMC}$),
Δq_{heat} is the modification of the given heat flux boundary,
$(\sum E)_{incidence}$ and $(\sum E)_{reflection}$ are the summed up incident and reflected energy fluxes of molecules hitting the surface, which can be obtained from DSMC simulation,
A is the area of the collision surface.

2.2.5. Convection heat transfer between the glass envelope and the environment

For the heat loss outside the glass envelope to the atmosphere, the convection heat transfer is the major one, especially when wind is blowing. From Newton's law of cooling,

$$q_{5-6,conv} = h_5 \pi D_5 (T_5 - T_6) \tag{23}$$

$$h_5 = \frac{\lambda_6}{D_5} Nu_{D5} \tag{24}$$

Local Nusselt number distribution around the glass envelope is determined for each wind velocity and presented in Fig. 6, which is from the experimental measurements of Scholten and Murray [31].

For the radiation transfer between the glass envelope and sky,

$$q_{5-7,rad} = \varepsilon_5 \sigma \pi D_5 (T_5^4 - T_7^4) \tag{25}$$

where T_7 is the sky temperature and is taken as 290.15 K [6].

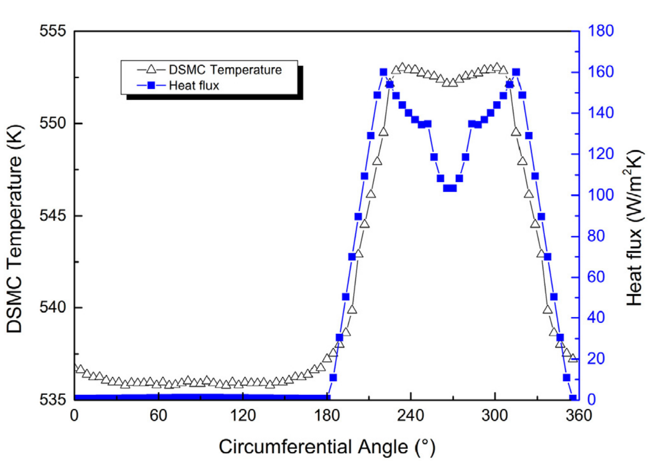

Fig. 5. Distribution of the non-uniform heat flux and temperature.

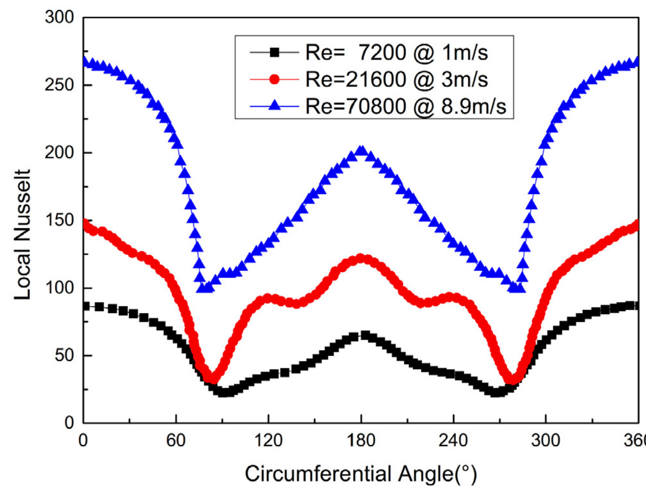

Fig. 6. Distribution of the local Nusselt number outside the envelope.

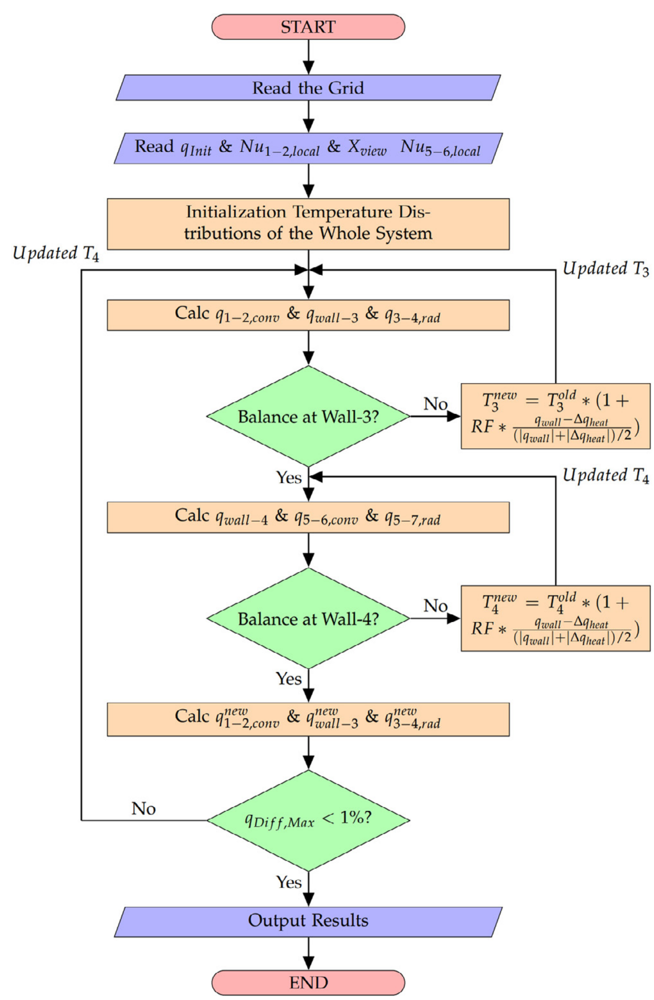

Fig. 7. The flowchart of the coupled method for the PTC.

2.2.6. Flowchart

The general computational algorithm is shown in Fig. 7. The entire heat transfer process is calculated by the following steps:

(1) According to the initial temperature of the wall boundary $T_{wall\text{-}3}(\theta)^{old}$, get the statistical heat flux $q_{wall\text{-}3}(\theta)$ by calling DSMC function through Eq. (22), calculate $q_{1-2,conv}(\theta)$ by

using Eqs. (1)–(4), calculate $q_{3-4,rad}(\theta)$ from Eqs. (8)–(17), and then calculate the energy balance at wall-3 by the following equation:

$$\Delta q_{heat}(\theta) = q_{Init}(\theta) - q_{1-2,conv}(\theta) - q_{3-4,rad}(\theta)$$

(2) If energy is not balanced at wall-3 (the outer surface of absorber tube), i.e., $\Delta q_{heat}(\theta)$ is not zero, substitute $q_{wall\text{-}3}(\theta)$ and $\Delta q_{heat}(\theta)$ obtained in the previous step into Eq. (20) to get $T_{wall\text{-}3}(\theta)^{new}$
(3) Update the boundary temperature $T_{wall\text{-}3}(\theta)^{new}$, repeat step 1 until energy is balanced at wall-3;
(4) Use the same method to get the energy balance at wall-4 (the inner surface of glass) by update the $T_{wall-4}(\theta)^{new}$ with Eq. (21);
(5) Refresh $q_{1-2,conv}(\theta)$ and $q_{3-4,rad}(\theta)$ with $T_{wall\text{-}4}(\theta)^{new}$. Repeat the whole iterations until the max difference from the old values is less than 1%.

The above calculation process is for the cross-sectional heat transfer. In the actual solar power field, the temperature of the heat transfer fluid gradually increases along its flow direction. The increase in the fluid temperature may have some effects of the heat transfer of the PTC. And the interest of an engineering design of a receiver is in the outlet temperature of HTF after axially going through a certain amount of PTC tube length. The above mentioned simulation procedure may be regarded as the representatives for a short length of PTC. Within the short length, the temperature increment of HTF is small. In order to get the outlet HTF temperature after going through, say 1000 meters of PTC, in the present study total ten cases are investigated, as shown in Table 2. The differences between different cases are mainly on the inlet fluid temperature and velocity. As shown in Table 2, from Case 5 to Case 10 the differences are in the fluid inlet temperature. Here different cases may represent different position of the PTC in the entire solar power field. And for the parameter shown in Case 8, four cases (Cases 1–4) are studied to investigate the effect of the HTF inlet velocity.

In this paper, a simplified 3-D model is constructed for the entire calculation process as follows. First cases with different HTF inlet temperature are simulated by the 2D model mentioned above, from which the PTC efficiency variation with HTF temperature can be fitted. In the axial direction 1-D model is used for the HTF temperature by using this fitted efficiency equation to get the outlet HTF temperature for a given condition.

In the following, the results of cross-sectional simulation for different cases will be discussed, and then the axial HTF temperature variation will be provided. In the presentation, whenever necessary the case number will be referred for the simulated results.

3. Results and discussion

3.1. Validation of view factor and DSMC model

Fig. 8(a) shows the view factor distribution at some cell-i on the surfaces and $\sum X_{3,4} = 1$. The number of cells on the surfaces is 180, for point i on wall-3, there are 53 cells on wall-4 would get the radiation energy from cell-*i*. When $T_3 = 500$ K and $T_4 = 322.7$ K, the radiative heat exchange rate simulated by cell to cell model is $E_{3\_X_{34}} = 85.76$ W and that from Eq. (7) is $E_{3\_equation} = 85.72$ W. The tiny difference of the two calculated results means view factor model is correct. Fig. 8(b) shows the effects of non-uniform heat flux on the self-radiation E_{3i}. The non-uniform heat flux causes about ±13.5% offset of local self-radiation in spite of the little difference of total self-radiation.

Table 3 compares the heat losses between the DSMC and experimental data. Our simulation is conducted according to the given uniform wall temperatures in [32] and the agreement is quite good.

3.2. Cross-sectional temperature distributions

Fig. 9 shows the differences between the cross-sectional temperature distributions from non-uniform condition and uniform heat flux condition for 1 Pa of the annulus pressure with the same average heat flux. It can be seen that the non-uniform heal flux makes the temperatures of the lower half tube significantly higher than that of uniform heat flux situation. For the case studied the maximum temperature of the lower part of PTC for non-uniform situation is 553.0 K, while that of the uniform situation is only 542.6 K. Compared with the temperature difference at the gap, the temperature differences of the others region shown in Fig. 2 are much small.

The effect of gas pressure on the cross sectional temperature distribution is shown in Fig. 10 with non-uniform heat flux distribution. It can be seen that with the increase of the annulus pressure, the influence of non-uniform heat flux on the temperature contours decreases. Since non-uniform heat flux distribution given in Fig. 5 is the normal situation, in the following presentation of results this will not be restated for simplicity.

Fig. 11 shows that the temperature distributions of the absorber tube and the glass envelop for case 10. It can be observed that the outside surface temperature distribution of the absorbed tube quite similar to the heat flux distribution with the maximum wall temperatures sit aside from the vertical line by about 50 degrees. However, for the glass envelope this non-uniformity is largely reduced and the circumferential temperature difference (CTD) of the glass envelop is much lower than that of the absorber tube (23.1 K vs. 45.8 K).

Table 2
Ten cases of simulation.

	Therminol VP-1 (HTF)						Solar heat flux	Air		Annulus
	ρ (kg/m^3)	k (W/(m·K))	c_p (kJ/(kg·K))	ν 10^6	T_{in} (K)	V_{in} (m/s)	q (W/m^2)	T_∞ (K)	V_∞ (m/s)	P (Pa)
Case 1	877	0.107	2.154	0.348	513.15	0.861	940	298.15	1.0	0.1
Case 2	877	0.107	2.154	0.348	513.15	1.722	940	298.15	1.0	0.1
Case 3	877	0.107	2.154	0.348	513.15	2.583	940	298.15	1.0	0.1
Case 4	877	0.107	2.154	0.348	513.15	3.444	940	298.15	1.0	0.1
Case 5	1007	0.129	1.747	1.111	363.15	2.583	940	298.15	1.0	0.1
Case 6	965	0.123	1.886	0.665	413.15	2.583	940	298.15	1.0	0.1
Case 7	922	0.115	2.021	0.460	463.15	2.583	940	298.15	1.0	0.1
Case 8	877	0.107	2.154	0.348	513.15	2.583	940	298.15	1.0	0.1
Case 9	828	0.098	2.287	0.281	563.15	2.583	940	298.15	1.0	0.1
Case 10	773	0.089	2.425	0.239	613.15	2.583	940	298.15	1.0	0.1

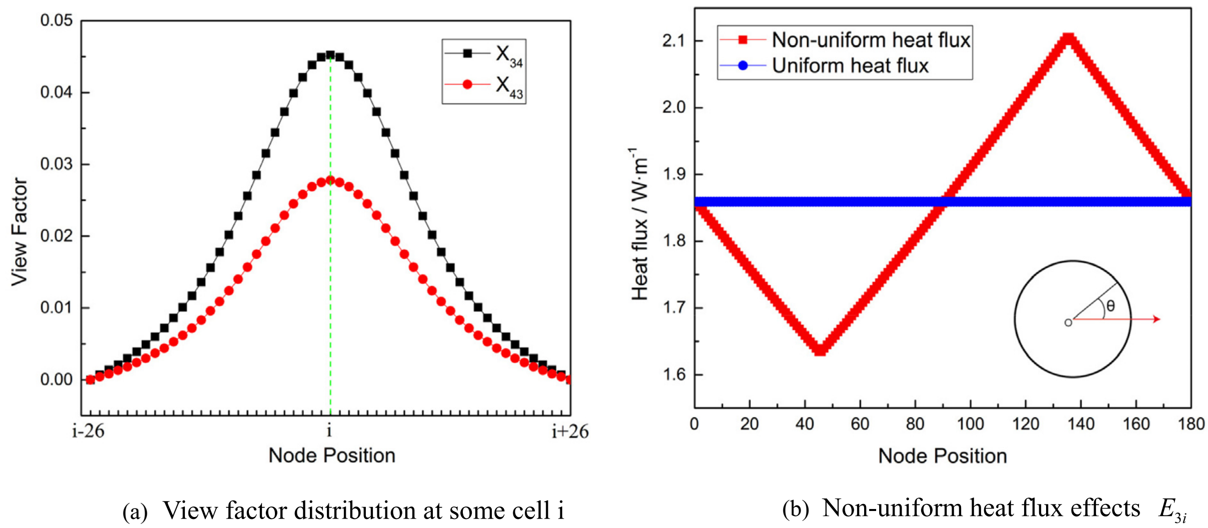

Fig. 8. Validation of view factor model.

Table 3
DSMC verification.

Pressure (Pa)	DSMC (W/m^2)	Experimental [32] (W/m^2)	Error
2.5	237.9	215.5	10.4%
5.0	484.2	509.0	−4.9%
50.	2978.5	3110.0	−4.2%

Convection heat transfer around the PTC can be considered as forced convection cross flow around a single horizontal cylinder. The wind speed effect of the glass envelop temperature is showed in Fig. 12. The maximum temperature and the CTD at wing speed of 3 m/s are 361.1 K and 42.6 K respectively, which are appreciably lower those at wind speed of 1 m/s, 363.1 K and 23.9 K respectively.

3.3. PTC tube efficiency

Come here the PTC heat loss, PTC efficiency and its influencing factors are discussed.

The effect of the annulus gas pressure on the PTC heat loss is presented in Fig. 13, where results for both uniform and non-uniform heat flux situations are shown. It can be seen that with the decrease in gas pressure the heat loss reduces very quickly when gas pressures are in the regions of 1–10 Pa. Below 1 Pa the gas pressure effect becomes mild and below 0.1 Pa the gas pressure almost has no effect at all. Especially in the region of 0.05–0.01 Pa the vacuum does not make any further contribution to the reduction of PTC heat loss. Thus for the engineering design purpose the vacuum of the annual gap of a PTC may be controlled below 0.1 Pa. It is to be noted that the non-uniformity of the periphery heat flux has some negative effect on the PTC efficiency only when the gas pressure is larger than 1 Pa, beyond which the effect of non-uniformity of heat flux can be neglected.

Fig. 14(a) shows the effect of the coating emissivity on the radiative heat loss in the annulus with two constant wall temperatures of the annual shown in the figure. From the figure it can be seen that radiative heat loss increases almost linearly with the increases of the emissivity of coating. Fig. 14(b) shows the effect of variable coating emissivity (variation of coating emissivity is determined according to the equation given in Table 1). Obviously when the temperature of HTF increases the annual wall temperatures will also increase. In Fig. 14(b) the variations of T_3 and T_4 with HTF temperature are specified. The situations of constant emissivity and variable emissivity are simulated. It can be seen that if there is a temperature-independent low emissivity of coating

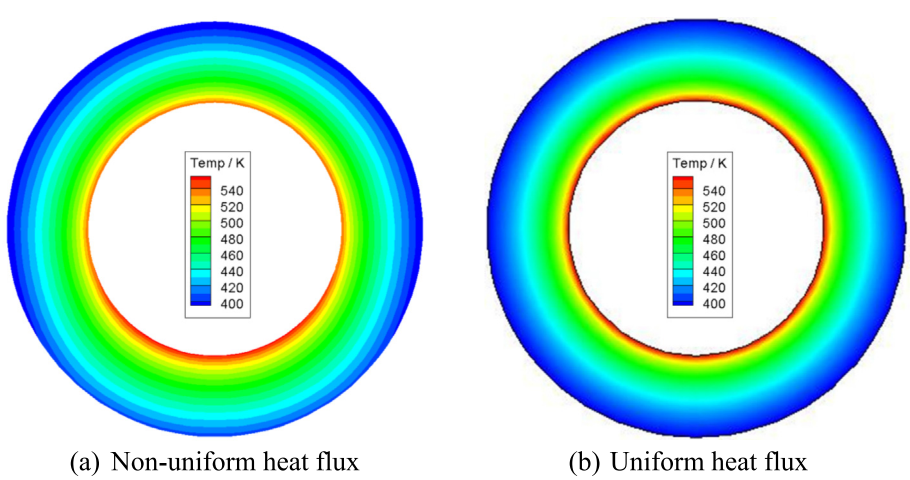

Fig. 9. Non-uniform heat flux effects on temperature distribution at 1 Pa.

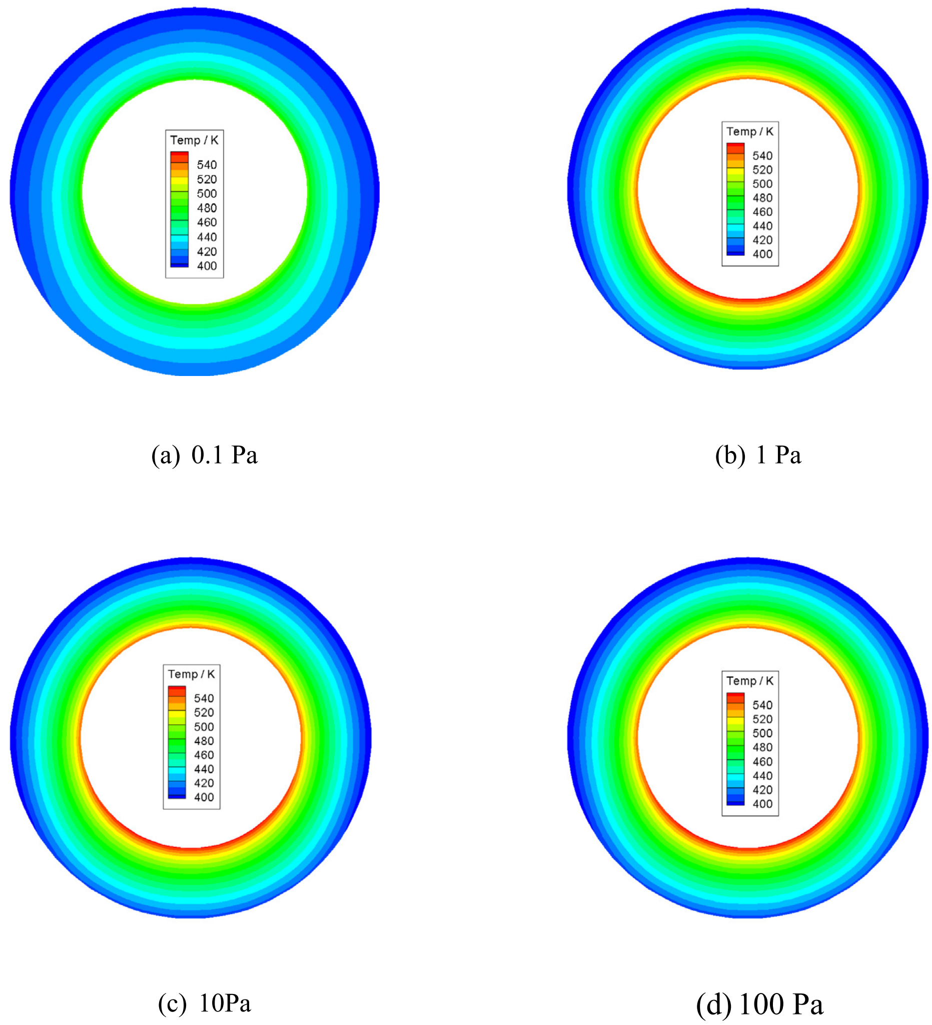

Fig. 10. Pressure effects on temperature contours.

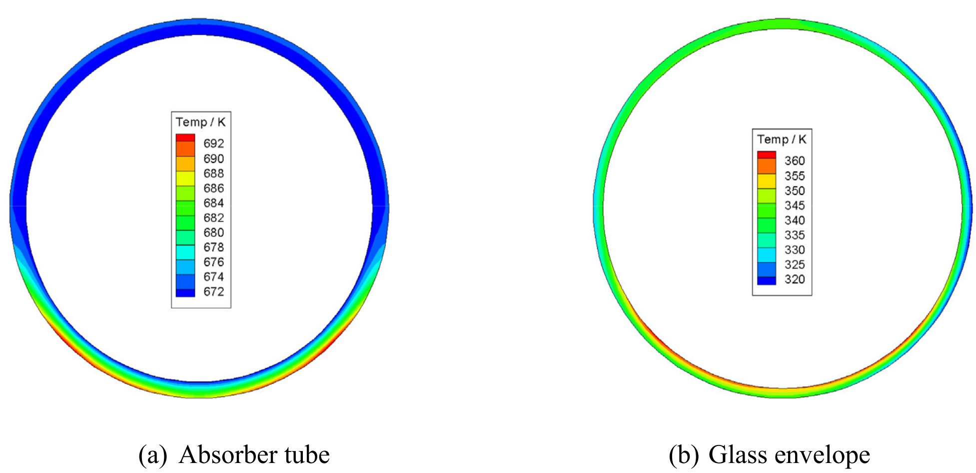

Fig. 11. Temperature contours of Case 10.

(constant low emissivity of 0.065 at T_3 = 398 K is given in [33]), the radiative heat loss can be reduced by half compared with the current variable coating. Actually, by using computer-aided optical design software, a multilayer solar-selective coating with the emittance of 0.070 at 450 °C was developed in [34]. The multilayer coating is the possible approach to realize the radiative heat loss reduction at high temperature.

The effect of the envelop diameter on the heat losses is presented in Fig. 15. As diameter of the glass envelop increases with other dimension remained the same, the distance between the

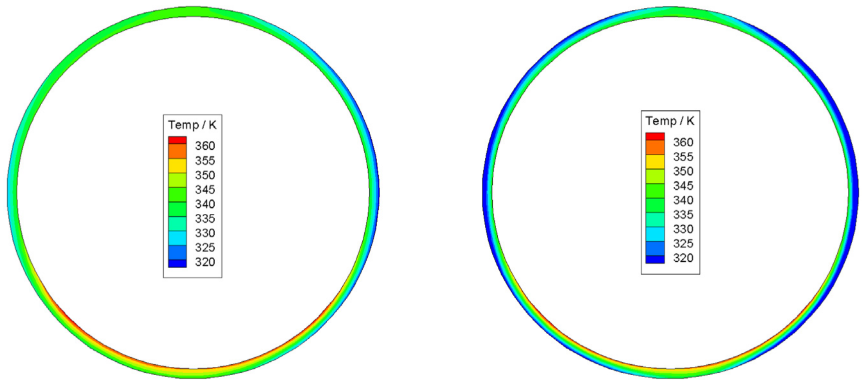

(a) Wind speed = 1 m/s (b) Wind speed = 3 m/s

Fig. 12. Temperature contours of glass envelop with different wind speed.

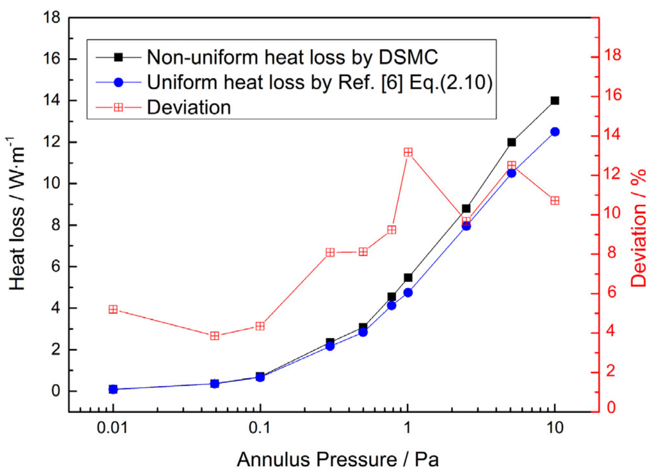

Fig. 13. Heat losses vs. pressures in the gap.

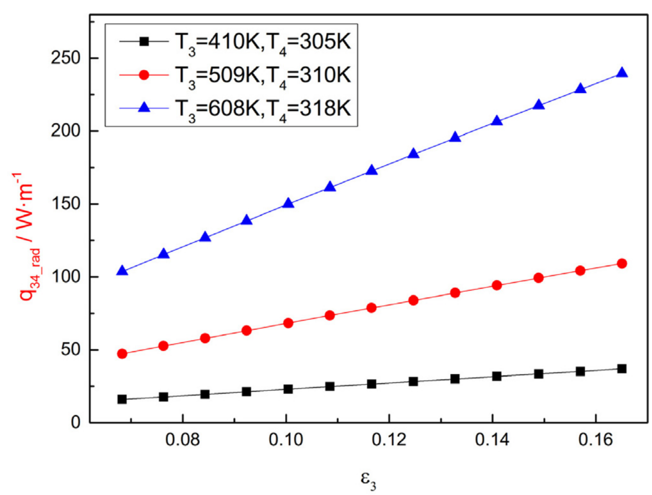

(a) Radiative heat loss vs emissivity (case 10)

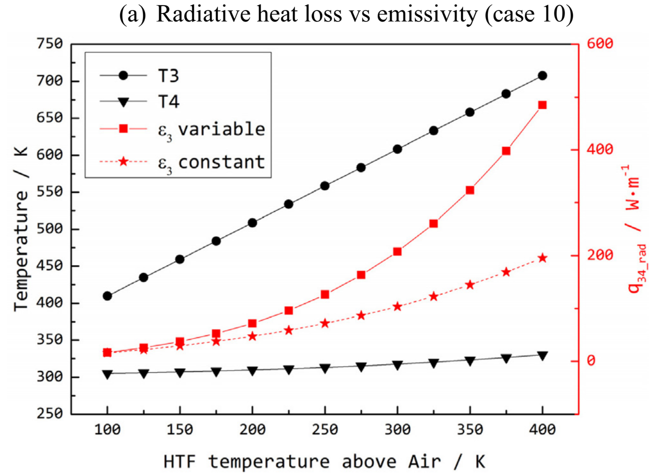

(b) Radiative heat loss vs emissivity (case 10)

Fig. 14. Radiative loss in the annulus comparing different emissivity of coating.

absorber tube and the envelop increases, which will decrease the glass temperature, leading to some decrease in the temperature difference between envelope outside wall and the ambient. On the other hand, the heat transfer area of the envelope increase linearly with the diameter which will increase the heat loss from the envelope to the environment. The final balance between the two opposite factors makes the heat loss being increased with diameter as shown in the figure. Thus the diameter of the envelop of a PTC should be small and the lower limitation is controlled by the strength of the tube, as the absorber tube will slightly bow when heated.

Fig. 16 shows the PTC efficiency data obtained by the above coupling algorithm, according to the parameters of Case 8 in Table 2 for different HTF temperature with HTF's physical property changes being considered. As it can be expected that at a higher HTF temperature, the efficiency of PTC will drop. The simulated data in Fig. 16 can be well fitted by Eq. (26):

$$\eta = 0.747 - 0.00679 * e^{\frac{T_1 - 273.15 - 84.86}{129.86}} \quad (26)$$

where T_1 is the HTF temperature.

3.4. Axis-wise variation of HTF temperature

Come here the efficiency equation is adopted for 1-D computation of the HTF temperature variation along the tube axis. For an entire length of several hundred meters of PTC, one meter is taken as a unit, and with a given inlet HTF temperature its outlet temperature can be computed by the efficiency equation with given solar radiation and other environmental conditions. The HTF outlet temperature is taken as the inlet one for the next unit and the

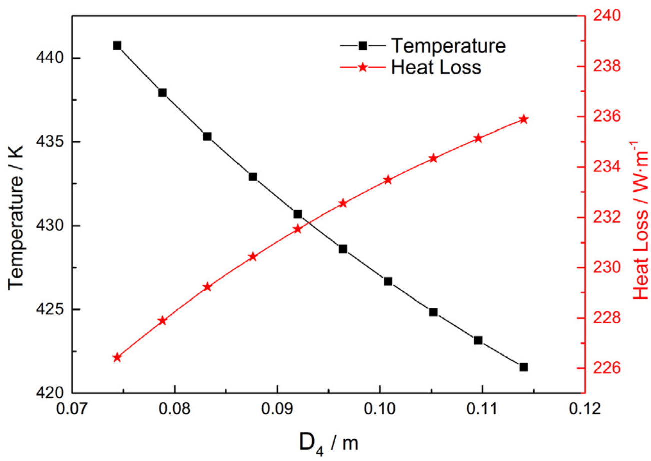

Fig. 15. Effect of the envelop size on the heat losses (Case 10).

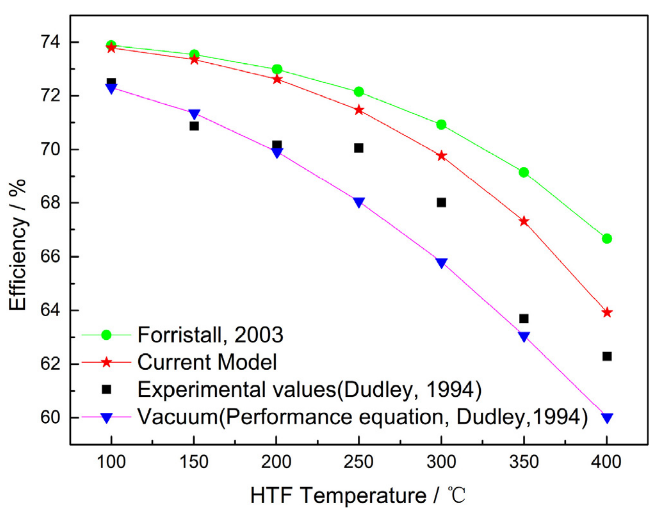

Fig. 16. PTC efficiency vs HTF temperatures.

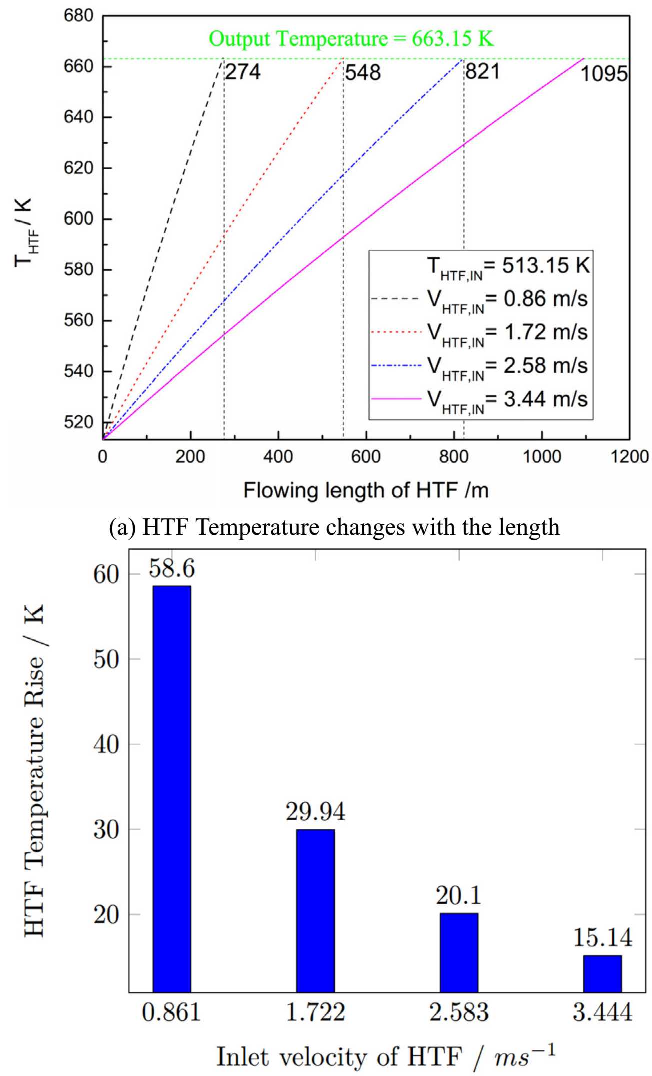

(a) HTF Temperature changes with the length

(b) HTF Temperature raised per 100 m tube

Fig. 17. HTF temperature results of Cases 1–4.

same computation is repeated. In conjunction with the 2D cross-sectional model a simplified 3D model is thus constructed for the HTF temperature with enough accuracy, which is the major concern for the design of a PTC receiver.

Figs. 17 and 18 show the 1-D HTF temperature changes with the length in the absorber tube with HTF's physical property changes with temperature being considered. Fig. 17 shows the effect of inlet velocity with fixed HTF outlet temperature and inlet temperature. The inlet velocity of 2.583 m/s (=140 gpm) adopted in Fig. 17 is the standard HTF flow rate and the total length of KJC test-loop is 779.52 m according to [6]. From Fig. 17, HTF temperature raised 58.6 K with the inlet velocity of 0.861 m/s and only 15.1 K with the inlet velocity of 3.444 m/s after passing the first 100 m absorber tube. The required length of PTC for the four inlet velocities are 274, 548, 821 and 1095 m, respectively. So the deviation between the predicted required total length for the conditions of KJC test-loop and the actual total length is 5%. Since the heat transfer resistance between HTF and the inner surface of the absorber tube is very small compared with other components, the increase of inlet velocity does not make benefit but increases significantly the total length of PTC, not to say the significant increase in the pumping power. Fig. 18 presents the effect of inlet HTF temperature with fixed HTF outlet temperature and inlet velocity. From Fig. 18, HTF temperature raises 22 K with the inlet temperature of 363.15 K and 19.54 K with the inlet temperature of 613.15 K after passing the first 100 m absorber tube. To reach the specified outlet HTF temperature the required total lengths of PTC for the six inlet temperatures are, respectively, 262, 537, 821, 1110, 1399 and 1689 m. It can be seen that the require PTC length is approximately proportional to the total temperature rise of HTF. The decrease of efficiency with the increase of HTF temperature makes such increase non-linear.

The best engineering design should give the shortest PTC tube length for a given thermal load. By inserting a medium storage tank, HTF could flow at a high velocity (e.g. 2.583 m/s) in the low temperature working segments, whereas at a low velocity (e.g. 0.861 m/s and in 3 parallel absorber tube to keep the same flow rate) in the high temperature working segments. The combination of two running velocity needs only 744 meters of total lengths of PTC to reach the specified outlet HTF temperature, relative to 821 meters of total lengths of PTC with the inlet velocity of 2.583 m/s.

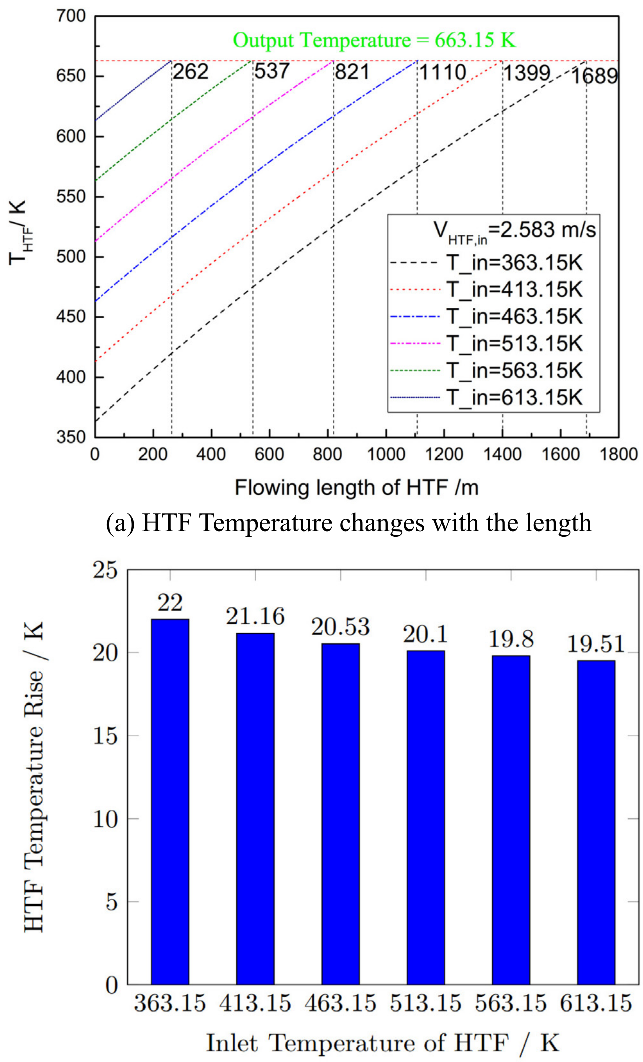

(a) HTF Temperature changes with the length

(b) HTF Temperature raised per 100 m tube

Fig. 18. HTF temperature results of Cases 5–10.

4. Conclusions

In this paper, the performance of the PTC system using Therminol VP-1 as the HTF was numerically studied. Following conclusions can be made:

(1) A fully coupled simulation algorithm for the cross-sectional heat transfer in a PTC is presented, which includes many practical factors affecting PTC efficiency into considerations, such as the non-uniform periphery heat flux distribution, the variable pressure in vacuum gap, and the periphery-variable local heat transfer coefficient of the envelope. The new coupling algorithm can be used to optimize the parameters of a PTC tube.

(2) A simplified 3D model is proposed to determine the axial variation of HTF temperature with enough accuracy. The major idea of this model is that 2D cross-sectional CFD simulation is first conducted by the proposed algorithm to obtain the PTC efficiency at different HTF temperature. The simulated efficiency data are then fitted. The fitted equation is used to compute the HTF axial temperature increase for a small length unit with given inlet HTF temperature. Such computation is repeated until the final length is reached. The simplified 3-D model can be used for preliminary design of a PTC receiver.

(3) Simulation results show that the gas pressure in annulus has significant effect on the PTC heat loss. However, when it reduces to 0.1 Pa, further increase in vacuum does not make any contribution for the heat loss reduction.

(4) Effects of coating emissivity and envelope diameter are analyzed. Reduction of emissivity and envelope diameter have positive effect for heat loss reduction, with the effect of emissivity being more significant.

(5) The HTF inlet velocity has significant effect on the total PTC length to reach a certain value of its outlet temperature. Since the heat transfer resistance of HTF is not the major component, the HTF velocity is recommended not large.

(6) An operation scheme is proposed that HTF should flow at a high velocity in the low temperature working segments, whereas at a low velocity in the high temperature working segments. By appropriate combination of HTF velocities at different temperature region the total length of the PTC tube to reach a certain amount of thermal load may be reduced.

Acknowledgments

The present study is supported by National Natural Science Foundation of China (Grant number 51136004) and the 111 Project (B16035).

References

[1] Y.L. He, D.H. Mei, W.Q. Tao, W.W. Yang, H.L. Liu, Simulation of the parabolic trough solar energy generation system with Organic Rankine Cycle, Appl. Energy 97 (2012) 630–641.
[2] Z.D. Cheng, Y.L. He, J. Xiao, Y.B. Tao, R.J. Xu, Three-dimensional numerical study of heat transfer characteristics in the receiver tube of parabolic trough solar collector, Int. Commun. Heat Mass Transfer 37 (7) (2010) 782–787.
[3] K. Wang, Y.L. He, Z.D. Cheng, A design method and numerical study for a new type parabolic trough solar collector with uniform solar flux distribution, Sci. China Technol. Sci. 57 (3) (2014) 531–540.
[4] C. Kutscher, F. Burkholder, J.K. Stynes, Generation of a parabolic trough collector efficiency curve from separate measurements of outdoor optical efficiency and indoor receiver heat loss, J. Sol. Energy Eng. 134 (1) (2012) 011012.
[5] V.E. Dudley, G.J. Kolb, M. Sloan, D. Kearney, SEGS LS2 Solar Collector – Test Results Report of Sandia National Laboratories SANDIA94-1884, 1994.
[6] R. Forristall, Heat Transfer Analysis and Modeling of a Parabolic Trough Solar Receiver Implemented in Engineering Equation Solver, National Renewable Energy Laboratory, 2003.
[7] J. Lu, J. Ding, J. Yang, X. Yang, Nonuniform heat transfer model and performance of parabolic trough solar receiver, Energy 59 (2013) 666–675.
[8] J. Wang, X. Huang, G. Gong, M. Hao, F. Yin, A systematic study of the residual gas effect on vacuum solar receiver, Energy Convers. Manage. 52 (6) (2011) 2367–2372.
[9] Y.J. Wang, Q.B. Liu, J. Lei, H.G. Jin, A three-dimensional simulation of a parabolic trough solar collector system using molten salt as heat transfer fluid, Appl. Therm. Eng. 70 (1) (2014) 462–476.
[10] J. Muñoz, A. Abánades, Analysis of internal helically finned tubes for parabolic trough design by CFD tools, Appl. Energy 88 (11) (2011) 4139–4149.
[11] Y.-L. He, J. Xiao, Z.-D. Cheng, Y.-B. Tao, A MCRT and FVM coupled simulation method for energy conversion process in parabolic trough solar collector, Renewable Energy 36 (3) (2011) 976–985.
[12] Z.D. Cheng, Y.L. He, F.Q. Cui, R.J. Xu, Y.B. Tao, Numerical simulation of a parabolic trough solar collector with nonuniform solar flux conditions by coupling FVM and MCRT method, Sol. Energy 86 (6) (2012) 1770–1784.
[13] S.M. Jeter, Calculation of the concentrated flux density distribution in parabolic trough collectors by a semifinite formulation, Sol. Energy 37 (5) (1986) 335–345.
[14] R.V. Padilla, G. Demirkaya, D.Y. Goswami, E. Stefanakos, M.M. Rahman, Heat transfer analysis of parabolic trough solar receiver, Appl. Energy 88 (12) (2011) 5097–5110.
[15] Z. Tang, Z.X. Sun, Z.Y. Li, H.Y. Ling, W.Q. Tao, Numerical simulation of vacuum annulus in a parabolic trough solar collector (In Chinese), J. Eng. Thermophys. 34 (6) (2013) 1133–1136.

[16] X.P. Zhao, L.Z. Yao, Z. Tang, W.Q. Tao, DSMC Study on the rarefied gaseous heat transfer in annulus heated by nonuniform heat flux, in: Proceedings of the 15th International Heat Transfer Conference, IHTC15-08681, 2014.
[17] Y.B. Tao, Y.L. He, Numerical study on coupled fluid flow and heat transfer process in parabolic trough solar collector tube, Sol. Energy 84 (10) (2010) 1863–1872.
[18] X.W. Song, G.B. Dong, F.Y. Gao, X.G. Diao, L.Q. Zheng, F.Y. Zhou, A numerical study of parabolic trough receiver with nonuniform heat flux and helical screw-tape inserts, Energy (2014).
[19] M. Roesle, P. Good, V. Coskun, A. Steinfeld, Analysis of conduction heat loss from a parabolic trough solar receiver with activevacuum by Direct Simulation Monte Carlo, Numer. Heat Transfer A 62 (5) (2012) 432–444.
[20] N. Naeeni, M. Yaghoubi, Analysis of wind flow around a parabolic collector (1) fluid flow, Renewable Energy 32 (11) (2007) 1898–1916.
[21] N. Naeeni, M. Yaghoubi, Analysis of wind flow around a parabolic collector (2) heat transfer from receiver tube, Renewable Energy 32 (8) (2007) 1259–1272.
[22] A.A. Hachicha, I. Rodriguez, J. Castro, A. Oliva, Numerical simulation of wind flow around a parabolic trough solar collector, Appl. Energy 107 (2013) 426–437.
[23] A.A. Hachicha, I. Rodríguez, A. Oliva, Wind speed effect on the flow field and heat transfer around a parabolic trough solar collector, Appl. Energy 130 (2014) 200–211.
[24] S.M. Yang, W.Q. Tao, Heat Transfer (in Chinese), fourth ed., Higher Education Press, Beijing, Beijing, 2006.
[25] J.R. Davis, Alloy Digest Sourcebook: Stainless Steels, ASM International, 2000.
[26] W.Q. Tao, Numerical Heat Transfer, Xi'an Jiaotong University Publication, Xi'an, 2001.
[27] G.A. Bird, J. Brady, Molecular Gas Dynamics and the Direct Simulation of Gas Flows, Clarendon Press, Oxford, 1994.
[28] J. Thomas, Heat Conduction in Partial Vacuum, NASA STI/Recon Technical Report N, 80 (1979) 25618.
[29] G.A. Bird, J.M. Brady, Molecular Gas Dynamics and the Direct Simulation of Gas Flows, Clarendon Press, Oxford, 1994.
[30] H. Akhlaghi, E. Roohi, S. Stefan, A new iterative wall heat flux specifying technique in DSMC for heating/cooling simulations of MEMS/NEMS, Int. J. Therm. Sci. 59 (2012) 111–115.
[31] J. Scholten, D. Murray, Unsteady heat transfer and velocity of a cylinder in cross flow—i. Low freestream turbulence, Int J. Heat Mass Transfer 41 (10) (1998) 1139–1148.
[32] H. Chalabi, O. Buchina, L. Saraceno, M. Lorenzini, D. Valougeorgis, G.L. Morini, Experimental analysis of heat transfer between a heated wire and a rarefid gas in an annular gap with high diameter ratio, J. Phys. Conf. Ser. 362 (012028) (2012).
[33] T. Stuetzle, N. Blair, J.W. Mitchell, W.A. Beckman, Automatic control of a 30 MWe SEGS VI parabolic trough plant, Sol. Energy 76 (1) (2004) 187–193.
[34] C.E. Kennedy, Progress to Develop an Advanced Solar-selective Coating, National Renewable Energy Laboratory (NREL), Golden, CO, 2008.